Characterization of innovative Pt-ceria catalysts for PEMFC by means of *ex-situ* and *operando* X-Ray Absorption Spectroscopy

Simone Pollastri [a,d,*], Marco Bogar [a,b], Roman Fiala [a,c,f], Heinz Amenitsch [b],
Yurii Yakovlev [c], Alessandro Lavacchi [e], Giuliana Aquilanti [d],
Vladimir Matolin [c]

[a] CERIC-ERIC, Strada Statale 14 34149 Basovizza, Trieste, Italy
[b] Graz University of Technology, Institute for Inorganic Chemistry, Stremayrgasse 9, 8010 Graz, Austria
[c] Faculty of Mathematics and Physics, Charles University, Prague, Czech Republic
[d] Elettra - Sincrotrone Trieste S.C.p.A., SS 14 - km 163,5, 34149, Basovizza, Trieste, Italy
[e] Istituto di Chimica dei Composti Organometallici (CNR-ICCOM), Via Madonna del Piano 10, 50019, Sesto Fiorentino, Italy
[f] RadBee Technology s.r.o., Kokořov 8, 33501 Žinkovy, Czech Republic

HIGHLIGHTS

- 2 kind of Pt-ceria anode catalyst were prepared using a novel sputtering technique.
- Differences in the efficiency are visible in the first days of operation.
- Samples were studied both *ex situ* and *in operando* conditions through XAS and SAXS.
- When sputtered on Carbon Ionomer Layer, the catalyst is less stable.
- Pt^{2+} fraction increases as the Pt/Ce ratio decreases.

GRAPHICAL ABSTRACT

The lower efficiency and stability of Pt-ceria anode catalyst sputtered on Carbon-Ionomer-Layer has been linked to the quick reduction of Ce.

ARTICLE INFO
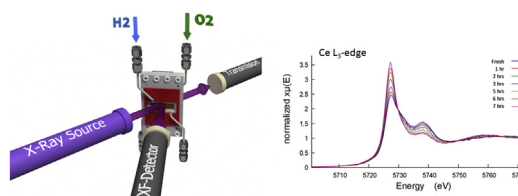
ABSTRACT

As the demand for energy is rising, the role of batteries and fuel cells in everyday life is undeniable, but fuel cell systems are still currently not employed worldwide mainly because of their cost, which is due to the large amount of Pt used in catalyst layers.

Recently, it was demonstrated that catalysts composed by low Pt loading (around 10 μg/cm^2) onto ceria (CeO$_x$) matrix are a promising alternative, showing comparable performances with respect to catalysts made by Pt only. Indeed, a strong metal to support

---

*   *Corresponding author.* CERIC-ERIC, Strada Statale 14 34149 Basovizza, Trieste, Italy.
    E-mail address: simone.pollastri@elettra.eu (S. Pollastri).

interaction between Pt and ceria has been already observed and exploited for application in direct methanol fuel cells.

In this context, the aim of the present study is to investigate the stability of innovative Pt-CeO$_x$ anode catalyst deposited on two different supports and characterized by means of X-ray Absorption Spectroscopy (XAS).

The XANES *ex-situ* data collected at the Ce L$_3$-edge highlighted the stability of ceria when directly deposited onto the nano-Gas Diffusion Layer (nGDL) whereas it is particularly unstable when deposited onto the so-called Carbon Ionomer Layer (CIL), where Ce was found irreversibly reduced to Ce^{3+} upon contact with the air. These behaviors are confirmed also by preliminary test experiments conducted in *operando* conditions, using a modified fuel cell designed on purpose. In addition, EXAFS data collected *ex-situ* at the Pt L$_3$-edge evidenced an increase in the fraction of Pt^{2+} as the overall amount of Pt (or the Pt/Ce ratio) is decreasing, in agreement with existing literature.

Our results provide an extended picture about characterization of Pt-CeOx catalyst, focusing on the effects of the hosting support, in order to improve the fabrication of more stable Membrane Electrode Assemblies (MEAs) with low Pt contents to be employed with PEMFCs.

Introduction

Polymer Electrolyte Membrane Fuel Cells (PEMFCs) [1] are among of the most promising candidates to power electric mobility and particularly automotive. PEMFC potential is due to their high energy conversion efficiency and power density, fast refuelling and easy/fast start-up even at low temperatures.

Despite the progresses achieved in the last decades, fuel cell systems have not yet been massively deployed and, so far, only few commercial applications in automotive are available, like the Toyota Miraj. The main obstacles to the diffusion of this technology are the cost and the stability [2]. Accordingly, the path towards the massive deployment of PEMFCs requires the overcoming of two significant technical challenges: i) the reduction in the use of Pt-group metals (PGMs) as catalyst and ii) catalyst durability. These two issues are closely related as the use of lower amount of PGMs catalyst usually produce a decrease in both performance and stability. State of the art systems employ carbon black supported Pt catalysts, a Pt loading from 200 to 400 μg/cm^2 (with most of the material used at the cathode) and roughly 50 μg/cm^2 at the anode [3]. However, such loadings are still large and impact much on the cost of the device. For this reason, some recent work investigated catalysts system with ultra-low metal loadings, ranging from 1 to 200 μg/cm^2 [4,5], acting both as anode, cathode or both electrodes. The Department of Energy of the US (DOE) has defined that the reasonable target is to achieve an overall Pt loading of fuel cells of 125 μg/cm^2 or less.

Concerning durability, DOE has defined a target for the light duty vehicle of 5000 hrs by 2025 and 8000 hrs by 2030; at present, durability is around 4000 hrs. As most of the Pt is employed at the cathode, much research has been [6] and is currently [7] devoted to the development of novel and more efficient Pt electrocatalyst for the oxygen reduction reaction. However, development of advanced anode catalyst with reduced amount of PGM and better CO tolerance is still of high importance and may also help in achieving the DOE targets. Indeed, several works are now focusing on the implementation of anode catalysts [8].

Catalysts composed of a ceria (CeO$_x$) support used as a matrix where platinum (Pt) atoms are encapsulated [9–11] are receiving a great deal of attention in the frame of automobile catalytic converters [12], which are currently consuming approximately 40% of the worldwide produced Pt [13]. The interest further extends to the water-gas-shift (WGS) reaction, being a key step in fuel processing for hydrogen generation [14]. Recently, a novel nanostructured Pt-CeO$_x$ material for fuel cell anode catalysts prepared via magnetron sputtering has been presented [15–18] and patented [19].

Pt^{2+}-CeO$_x$ thin films show an exceptionally high activity for the Hydrogen Oxidation Reaction (HOR) at the anode side of PEMFCs and high durability [16, 17, 20–22 and references therein], despite employing up to 100-time lower Pt load compared to standard Pt/C catalysts [17,21,23]. Thanks to these features, such materials can be considered a promising alternative technology for future large-scale applications.

Because of the low amount of Pt in the compound, the Pt ions can be considered as ionic dopant of the CeO$_x$ thin film matrix, as demonstrated in a recent work of Dvořak et al. [24]. By combining experimental and theoretical models, the authors illustrate in which way the Pt^{2+} dopants in Pt-CeO$_x$ catalysts become single ionized Pt atoms. This picture has been confirmed also by Yang et al. [25] and Flytzani-Stephanopoulos et al. [26].

Single-atom catalysts represent the new frontier in heterogeneous catalysis, with precious metals ultimately dispersed as single atoms [25,26] to maximize their utilization [27].

However, in order to optimize the efficiency and stability of this catalysts, it is crucial to identify the physical and chemical processes behind both their catalytic activity and degradation processes; for example, it is still unclear whether the single supported atoms are the effective active centres where catalytic reactions take place or not [28–30].

Thus, the catalytic activity of single atom catalyst was found to differ from the behaviour of the (well-established) materials working as surface catalysts, being a complex and dynamic process with single atom active centres evolving in response to the changes of reaction atmospheres [31,32].

In this context, the aim of present work is to investigate innovative Pt-ceria anode catalysts for applications in PEMFC focusing on X-Ray Absorption Spectroscopy (XAS) data, collected both *ex-situ* and in *operando* conditions. The study will address the catalyst stability depending on the different kind of hosting supports, which are nano-Gas Diffusion Layer (nGDL) and the so-called Carbon-Ionomer Layer (CIL).

Materials

The two set of samples investigated both *ex-situ* and *operando* are Pt-ceria anode catalysts whose performances have been already preliminarily characterized through X-ray Photoelectron Spectroscopy (XPS), Electron Energy Loss Spectroscopy (EELS), Scanning Electron Microscopy (SEM), High Resolution Transmission Electron Microscopy (HRTEM) and endurance tests. These data are presented in Fiala et al. (2011, 2015 and 2016) and Nováková et al. (2020) [15,22,33and34], respectively.

The catalyst layers have been sputtered simultaneously (Fig. 1) on two different supports to ensure the same loading, resulting in sample PtCeOx/CIL (PCC) sputtered on Carbon Ionomer Layer (CIL) and sample PtCeOx/nGDL (PCnG) sputtered on nano Gas Diffusion Layer (nGDL). In addition, catalyst samples deposited on CIL with and without ceria and different Pt loadings (1 or 10 μg/cm^2) were also investigated only *ex-situ* and named: Pt1μg; Pt1μgCeOx; Pt10μg; Pt10μgCeOx. Preparation methods and detailed description are provided below.

Sample preparation

The anode catalysts layers were prepared by magnetron sputtering on two different substrates: a commercial nGDL support (SGL TECHNOLOGIES GmbH, Sigracet GDL 29 BC, thickness 235 μm) and a carbon ionomer layer (CIL).

CIL was made by spraying a carbon-based ink on a Teflon substrate. The carbon ink was composed by 2 mg of Carbon nanopowder (<50 nm (BET), 99+% (CAS 7440-44-0) Sigma Aldrich) and Nafion® solution 5% Alfa Aesar (1:1 with C − mass ratio), dissolved in 20 ml isopropyl alcohol for a resulting carbon loading of 0.5 mg/cm^2. For carbon spraying, ExactaCoat from SONOTek was used. The estimated thickness, evaluated via mechanical measurements, is several micrometers (5 μm after drying). The catalyst layers were coated on the two different substrates by simultaneous sputtering from two magnetrons: Pt target (SAFINA, 99.99%, 101.6 × 2 mm) at DC mode and CeO$_2$ target (Kurt J. Lesker, 99.99%, 4" x 0.125") at AC mode using balanced magnetrons (TORUS®, Kurt J. Lesker) in argon atmosphere at 0.5 Pa. DC mode was powered by DC source (DC01BP, Kurt J. Lesker) at 5 W and AC mode was carried out with a AC power source (CESAR® RF generator (13.56 MHz) coupled with a NAVIO™ impedance matching device) at 80 W power.

Pre-sputtering pressure was 5×10^{-4} Pa. Sputtering rate was calibrated with measuring step between sputtered film and region with removed film on silicon wafer reference support using atomic force microscope (AFM). Calibration of the magnetrons by AFM together with XPS data allowed to estimate thickness and composition of sputtered PtCeO$_x$ layer for PCC, PCnG and Pt10μgCeO$_x$ samples; considering a Pt concentration in the composite film of 22% (±5%) and an overall thickness of 30 nm, the corresponding Pt loading was defined at about 10 μg/cm^2. Similarly, estimated thickness of samples Pt1μg, Pt1μgCeO$_x$ and Pt10μg are 0.5 nm, 3 nm and 5 nm, respectively.
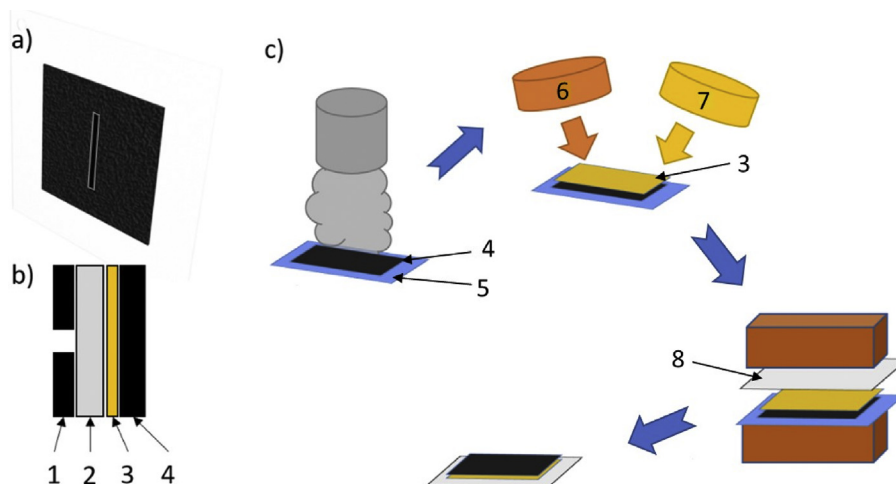
Fig. 1 − a) Membrane electrode assembly (MEA) with cut hole on cathode side. b) MEA cross section: (1) cathode catalyst layer with hole; (2) Nafion® NE1035; (3) sputtered anode catalyst layer; (4) support layer, that is carbon ionomer layer (CIL) for PCC samples and nGDL for PCnG samples. c) Anode fabrication for PCC sample: at first, carbon ink (4) is sprayed on Teflon support (5). Then, catalyst is deposited via magnetron sputtering (6 is CeO$_2$ target; 7 is Pt target) onto CIL. Finally, the catalyst layer is printed on Nafion® membrane (8) and, after Teflon removal, anode is ready to be used for composing the MEA. Concerning PCnG sample, catalyst was directly sputtered on nGDL and later assembled in MEA.

Finally, catalysts were printed onto a Nafion® membrane (NE1035, $C_7HF_{13}O_5S\cdot C_2F_4$), while supporting Teflon was removed; printing procedure was performed by hot press method at 120 °C and 2 MPa for 3 min. A scheme of the whole sample preparation procedure is presented in Fig. 1c.

Fuel cell design

Fig. 2 reports the assembly scheme of the PEMFC used for *operando* experiments. This cell has been specifically developed to be analysed both at the SAXS and XAFS beamlines of ELETTRA synchrotron (Trieste, Italy). The technical description of the cell will be the subject of another paper together with the SAXS results.

It is necessary to underline the innovative character of the cell and the fact that the measurements reported here represent the first attempt to use this prototype; for this reason, there were obviously drawbacks, which will be discussed in Section Operando XAS at the Ce and Pt L_3-edge.

The cathode was made by commercially available nGDL supported Pt/C catalyst (purchased from Alfa Aesar with Pt loading of 500 µg/cm^2, 60% Platinum on Vulcan - Carbon Paper Electrode). A small hole has been cut on the cathode along the X-ray path, in order to have the information of the local and electronic structure of the Pt exclusively present on the anode.

The cell was operated with pure fully hydrated hydrogen as fuel and oxygen as oxidant under atmospheric pressure. The flow rates of H_2 and O_2 were controlled at 140 ml/min and 110 ml/min, respectively.

The temperature of the cell as well as humidifier tanks were controlled at 65 °C. The performance of the Pt doped ceria anode was evaluated by comparing it with a reference anode tested at same FC working conditions. In the reference MEA the Pt doped ceria anode was replaced by the commercially available Pt/C catalyzed nGDL.

First XAS spectra were collected on the assembled PEMFC without gas flow and cable connection (defined "dry" initial state). Then gas lines were connected and wet nitrogen was used to warming up the cell and to hydrate the MEA for about 4 h, bringing internal relative humidity (RH) to about 100% ("wet" state).

After the membrane was completely hydrated, the hydrogen and oxygen gases were fluxed on the anode and cathode sides, with the cell in OCV state (open circuit voltage).

Then, the final step consisted of collecting spectra on the operating PEMFC @ 0.5 V ("05 V" state).

Experimental

Scanning electron microscopy

The morphology of the two kind of catalyst samples studied in the present paper was investigated by scanning electron microscopy (SEM). The SEM study was conducted using a Tescan MIRA 3 instrument available at the Faculty of Science of the Charles University in Prague, operating with an accelerating voltage of 30 kV. The samples were conductive so Au coating was not necessary and they were simply loaded on the sample holder.

Catalyst performance

To assess the performance of the anode catalyst, measurements in a standard fuel cell setup were conducted both to measure I–V curves and to check catalyst durability.

The membrane electrode assembly (MEA) was sandwiched in the graphite bipolar plates with a single serpentine flow field and active area of 4 cm^2. Fuel cell testing was performed after 24 h of the cell conditioning at a temperature of 65 °C and constant flow (50 sccm) of humidified N_2 on both fuel cell sides. After conditioning, anode and cathode catalysts were fed with fully hydrated hydrogen and oxygen (50/50 sccm), respectively. No back-pressure was used. For durability test, a constant voltage of 0.5 V was set by an electronic load (BK Precision 8500) and the current was recorded as a function of time. Polarization curves were measured by an electronic load (BK Precision 8500) after the break-in procedure. Measurements were performed in the current control regime. Current was step-wise increased by 20 mA per each step every 3 s, while voltage response was recorded.

Small angle X-ray scattering

To complete morphological characterization, small angle X-ray scattering (SAXS) patterns were recorded on freshly prepared samples at the SAXS beamline (ELETTRA, Trieste, Italy) [35]. Beam photon energy was set to 8 keV, corresponding to a wavelength λ = 0.154 nm.
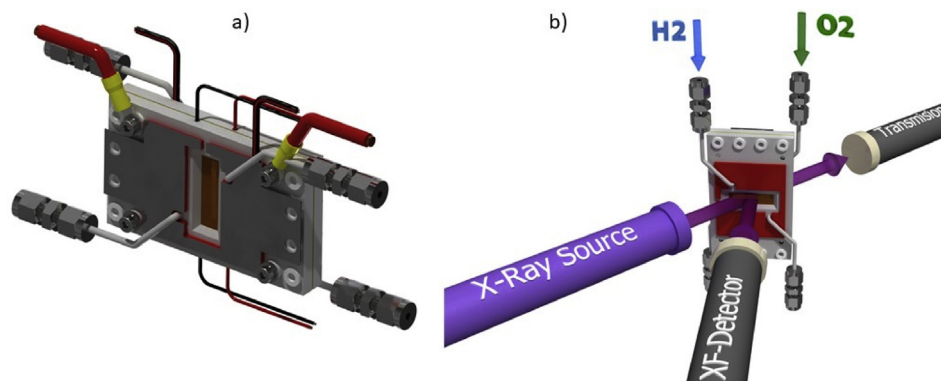

Fig. 2 – a) The assembled PEMFC with gas inlets and outlets, thermocouple and wires for voltage and current sense (cell dimension: 10 × 6 cm). b) Scheme of the experimental setup for *operando* XAS experiments at the XAFS beamline.

Silver behenate was used as a calibrant, with a sample to detector distance equal to 1512 mm. Scattering patterns were recorded from a 2D detector (Pilatus3 1 M, Dectris) and resulting two-dimensional images were azimuthally integrated to obtain a 1D pattern [36], further normalized to correct for transmission and intensity fluctuations.

Two models were used for fitting CIL/Nafion® (i.e. without the catalyst layer) and PCC samples. The former sample was fitted by using a power law and two Voigt peaks. The first term is describing diffused scattering produced from carbon porous structure, while the two peaks are used to model the ionomer peak and the matrix knee, characterizing the Nafion® scattering pattern [37].

In presence of the catalyst, a term to describe the scattering contributions produced from catalyst nanoparticles was added to the model. It was composed by the product of a form factor (which considers the size of the scattering objects) by a structure factor taking into account their displacement on the substrate. As a form factor, a set of spheres following the Schulz distributions was selected [38,39]. As a structure factor, the so-called Sticky-Hard Sphere model [40,41] was chosen.

X-ray Absorption Spectroscopy

Pt and Ce L_3-edge *operando* XAS spectra were collected at the XAFS beamline (ELETTRA, Trieste, Italy) [42] in fluorescence mode using fixed exit double crystal Si(111) monochromator.

Energy calibration was done by collecting simultaneously spectra of Pt metal foil or CeO_2 pellet and assigning the position of the first inflection point at 11564.0 and 5726.2 eV (+3.2 eV with respect to metal Ce, see Fig. 3) for Pt and Ce data, respectively. The reference samples were placed in a second experimental chamber after the sample and after the I1 ionization chamber. Higher order harmonics contamination was suppressed by detuning the second monochromator crystal.

Spectra of *ex-situ* samples were collected at room temperature both in air at the XAFS beamline and in high vacuum conditions at the XRF beamline (ELETTRA, Trieste, Italy) [43,44].

Additionally, the spectra of reference compounds CeF_3 (Sigma Aldrich, CAS 7758-88-5), $CeCl_3$ (Sigma Aldrich, CAS 7790-86-5), CeF_4 (Sigma Aldrich, CAS 10060-10-3), CeO_2 (Alpha Aesar, CAS 1306-38-3), Ce (Carlo Erba, CAS 7440-45-1), $PtCl_2$
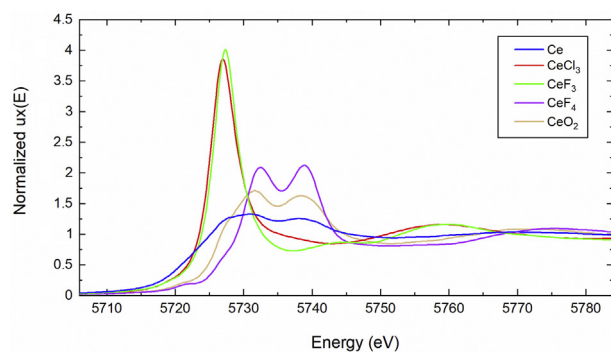
Fig. 3 – Normalized XANES spectra collected on reference Ce-bearing materials.

(Alpha Aesar, CAS 10025-65-7) and $PtO_2 \bullet nH_2O$ (Alpha Aesar, CAS 52785-06-5) were also collected. The normalized spectra of all the reference samples are reported in Fig. 3 and Fig. S1. Considering the high reactivity of metallic Ce in contact with the air, the sample container has been opened in an Ar-filled glove box, then the powder sample was sandwiched between two Kapton tapes and promptly placed in vacuum chamber for the XAS measurement.

For all the measurements, a variable energy step as a function of the energy was used: large step (5 eV) in the first 200 eV of the spectrum, smaller step (0.3 eV) in the XANES region and a k-constant step of 0.03 Å^{-1} in the EXAFS region. When the sample was not degrading, multiple spectra have been collected and merged in order to increase the signal to noise ratio. Merged spectra were then normalized with respect to the atomic background of the curve using the Athena software [45].

For selected spectra collected *ex-situ*, EXAFS refinements were also performed. Signals have been extracted using Athena, Fourier transformed with an Hanning window in the k range 3−12 Å^{-1} and quantitative analysis were carried out using the Artemis software (Demeter 0.9.25 package) [46].

The normalized XANES spectra of samples have been analysed through linear combination fitting (LCF) of spectra from the reference compounds, using the Athena software. CeF_3 was used to model the Ce^{3+} in CeO_x whereas CeF_4 and CeO_2 were used to model Ce^{4+} (detailed information in paragraph 4.3).

Results and discussion

### Morphological characterization

Results from scanning electron microscopy (SEM) are reported in Fig. 4: a) and c) show morphology of the CIL and of the commercial nGDL deposited on Teflon whereas b) and d) are CIL and nGDL layers coated with $PtCeO_x$ catalyst, respectively. It is not easy to spot the small differences among the samples with and without the catalyst because of its reduced thickness of about 30 nm. Nonetheless, from TEM investigations conducted previously on a set of samples prepared in the same way of our PCnG sample [22] is possible to distinguish the rough surface structure composing the carbon particles with respect to the catalyst coating, composed of Pt−ceria nano grains (Fig. 4e and f).

In order to reveal the catalyst particle morphology, SAXS measurements were also performed. The substrate porosity spotted from SEM images is reflected in the low q region of SAXS scattering patterns as well, which are represented in Fig. 5. Due to the small thickness of the CIL, Nafion® scattering pattern is still visible and the low amount of carbon is only revealed by an enhanced upturn at low q values. The fit of this trace was used to characterize the substrate hosting the catalyst layer.

From fitting the scattering pattern of the PCC sample, size and displacement of catalyst nanoparticles were retrieved: average particle diameter was found being equal to 8.42 ± 0.04 nm with a standard deviation of 0.20 ± 0.04 nm. In addition, minimum interparticle distance was retrieved being equal to 46.30 ± 0.62 nm.
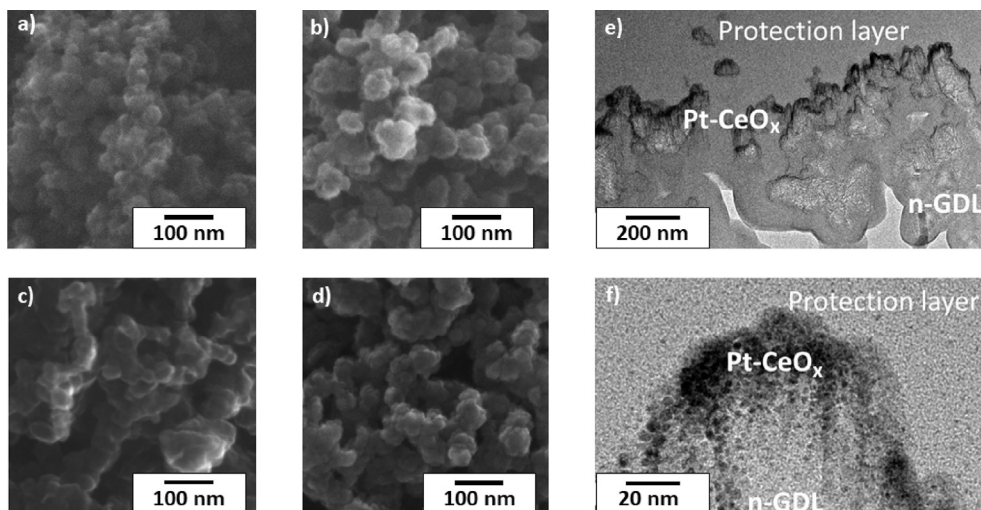
Fig. 4 − SEM images of: a) CIL layer as prepared; b) CIL layer coated by Pt-CeO$_x$ catalyst; c) nGDL; d) nGDL coated by Pt-CeO$_x$ catalyst. It can be observed that the sputtered catalyst layer creates a cauliflower-like structure, increasing the specific area of surface where reaction occurs. e) and f) are TEM images collected on PtCeOx/nGDL sample (from the work of Fiala et al. [22]).
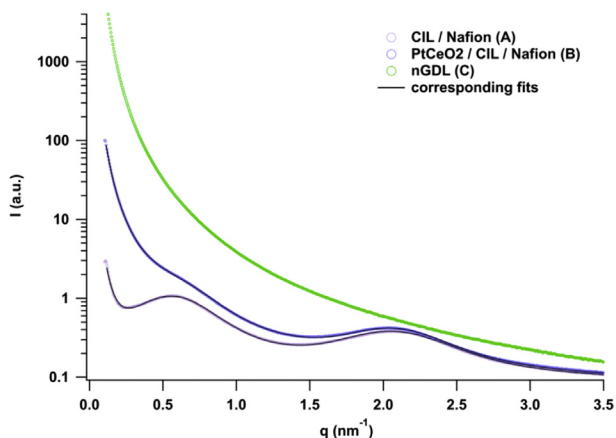
Fig. 5 − SAXS patterns recorded *ex situ* from nGDL and CIL/Nafion® supports and from PCC sample. By fitting the PCC trace it was possible retrieve information about catalyst morphology.

On contrary, the large amount of carbon constituting the nGDL is producing a very intense and broad diffused scattering pattern which does not allow to carry out further analysis. For this reason, scattering pattern from nGDL was not fitted and PCnG sample was not analysed through SAXS.

Catalyst performance

Performance of sputtered 30 nm PtCeO$_x$ layers on CIL and nGDL supports are shown in Fig. 6; time-dependent measurements are shown in Fig. 6a whereas I−V polarization curves are presented in Fig. 6b and c (respectively).

As can be seen, for both structures the current density decreases during the first 36 h and then stabilized at the same

value of 0.06 A/cm^2. Initial performance, however, was different with almost 2 times higher current density for nGDL based system. The I−V curves performance perfectly match with the measured values at the beginning of the durability test. The maximum power density for nGDL-supported catalyst reaches 0.45 W/cm^2, whereas for CIL is less than 0.22 W/cm^2. Presented curves showed no signs of mass polarization and twofold decrease of performance for CIL support could be the result of lower catalyst activity, as was previously suggested. Such results can be explained by differences in morphology and/or chemical changes of studied systems.

SEM images (Fig. 4a−d) showed the quite similar structure of supports, therefore, morphology cannot be a dominating factor defining performance. Moreover, both supports are based on carbon black particles, which are stable under the presented electrochemical environment. On the other hand, the presence of ionomer in CIL substrate can change the chemical structure of the catalyst layer. In a recent study [5], it has been showed that magnetron sputtering of CeO$_2$ on PFSA-based materials leads to a chemical reaction with significant ionomer etching. Change of chemical composition could result in catalysts with lower activity.

After prolonged testing, both systems showed the same, lower than the initial, performance. A decrease in the performance could be related to the restructuring of the composite catalyst, where platinum could aggregate into nanoclusters. Since the concentration of Pt in studied structures is the same, it can be concluded that the final morphology of Pt aggregates is similar.
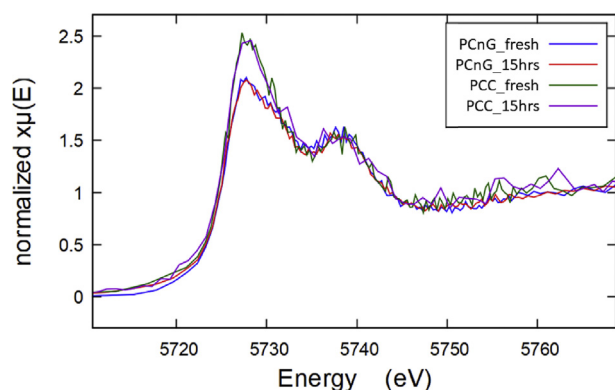
Ex-situ XAS at the Ce and Pt L$_3$-edge

At first, *ex-situ* XANES spectra at the Ce L$_3$-edge were collected on as prepared PCnG and PCC samples both in high vacuum and in air, in order to check for possible differences depending on the measurement conditions; the spectra are reported in Figs. 7 and 8, respectively. According to the spectra collected
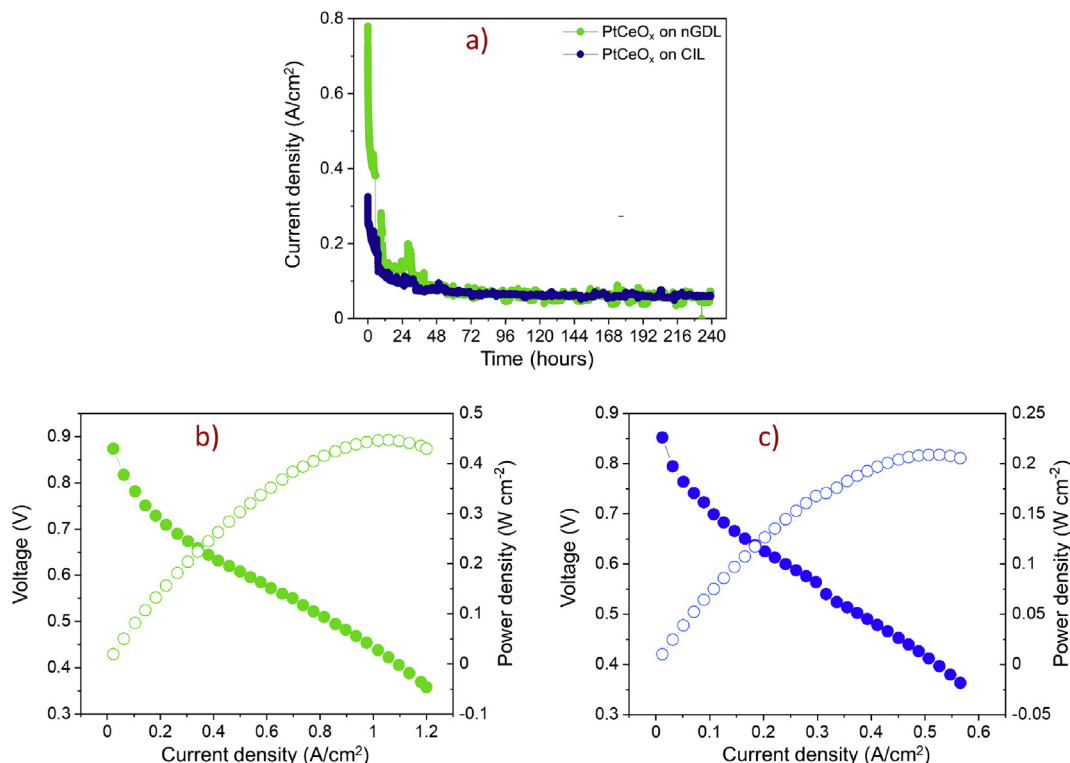
Fig. 6 − a) Performance of PtCeO$_x$ catalysts supported on nGDL (PCnG sample, green dots) and CIL (PCC sample, blue dots) measured in the FC operating with a voltage equal to 0.5 V. b,c) I−V polarization curves measured on PCnG and PCC samples (respectively). (For interpretation of the references to colour in this figure legend, the reader is referred to the Web version of this article.)
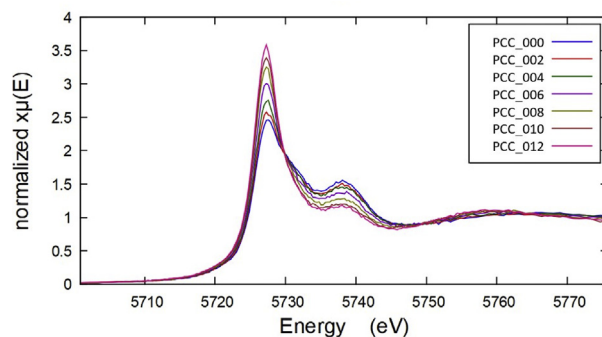
from reference Ce-bearing materials (Fig. 3), the intensity of the first peak (white line) on the Ce L$_3$-edge (at about 5727 eV) could be used to reveal and quantify the presence of Ce^{3+} by means of LCF analyses. In spectra measured in high vacuum (Fig. 7) is evident that the amount of Ce^{3+} is slightly higher in sample PCC and that both samples are stable over time.

When measured at room conditions, the spectral features characterizing PCnG did not show any variation over time (Fig. S5), analogously to what has been observed in vacuum. However, PCC shows a completely different behaviour. As visible in Fig. 8, the sample is reducing, incrementing the amount of Ce^{3+} over time, as underlined by the increase of the intensity of the white line. Since the sample was recorded outside from the environment of the PEMFC, this behaviour can be only due to its exposure to air. X-ray damaging was also considered as a possible explanation, but this thesis is denied by the stability observed on the same sample collected in high vacuum at XRF beamline (the photon flux density in the two beamlines is comparable).

Fig. 7 − Normalized Ce L$_3$-edge XANES spectra collected ex-situ in high vacuum (XRF beamline) on the freshly prepared samples PCC and PCnG (green and blue lines, respectively) and after 15 h (violet and red lines). (For interpretation of the references to colour in this figure legend, the reader is referred to the Web version of this article.)

Fig. 8 − Normalized Ce L$_3$-edge XANES spectra collected in air on the freshly prepared ex-situ sample PCC; spectra were collected every 35 min; the last one is after roughly 7 h.

LCF results (a typical fit is reported in Fig. S2 in the supplementary material) show that in both samples Ce is present both as Ce^{4+} (49% in PCC and 77% in PCnG) and Ce^{3+} (51% in PCC and 23% in PCnG) and that in just 7 hrs the amount of reduced Ce increases from 51% to 85% in PCC sample collected in air.

The quick reduction of dispersed ceria in presence of Pt in air at room conditions has been already observed by Wells et al. [47]. Despite the authors also indicate that Al_2O_3 is required to promote ceria reduction, our data demonstrate that its presence is not a necessary condition. Indeed, as can be seen in the Pourbaix diagrams for cerium in aqueous solutions reported by Hayes et al. (2002), Grulke et al. (2014) and by Channei et al. (2017) [48–50], at neutral pH with no difference of potential applied, the stable phase of cerium is Ce^{3+}.

In addition, Grulke et al. (2014) suggested that CeO_2 could be reduced to form Ce^{3+} salts in appropriate conditions, like "*the presence of different redox systems (such as ligands H_2O_2, O_2, H^+, e^-) which cause shifts in the phase equilibria between Ce^{3+} and CeO_2 (Ce^{4+}), as*" reported in the Pourbaix diagram; the reduction in presence of H_2O_2 and O_2 has also been reported by Yu et al. (2005) [51]. In our case, e^- could be available due to the Auger effect, which is however not a sufficient condition without water (as evidenced by the reproducibility of *ex-situ* XANES spectra collected in vacuum). We cannot however assess whenever the Ce^{3+} is in form of salts like CeF_3, $Ce(OH)_3$, Ce_2O_3 or other.

The instability of Ce in PCC samples could be related or to the hot press print of the catalyst layer on the Nafion® membrane and/or to the formation of Ce^{3+} in ionic form through the following reaction: $4Ce^{4+} + 2H_2O \rightarrow 4Ce^{3+} + 4H^+ + O_2$ [52].

This is not likely to happen in PCnG samples because of the higher stability (and low content, 5-10 wt%) of PTFE which is used to increase wettability of nGDL [53–55].

However, the key point is that both PCC and PCnG XANES spectra were collected using exactly the same experimental conditions in both beamlines, and hence the observed instability of ceria in PCC samples, opposite to the stability of PCnG ones, is already a precious indication that sputtering on CIL should not provide a stable and efficient anodic catalyst.

Complementary EXAFS results were obtained at the Pt L_3-edge on Pt catalyst samples sputtered on CIL in various amounts, with and without ceria. These measurements were performed prior to the investigation of Ce in PCC samples, and were intended for evaluating the data quality and collection times. For this reason, we were not aware of the instability of ceria in air and then in all the samples with Ce, this specie is completely reduced to Ce^{3+}.

The collected data are reported in Fig. 9 and Fig. S3 (FT EXAFS and XANES, respectively). These data revealed a trend according to the different Pt loading. More specifically, quantitative results derived from EXAFS refinements (Table 1) evidence a relative increase in the fraction of Pt^{2+} with respect to metallic Pt as the amount of Pt (or the Pt/Ce ratio) is decreasing.

This is also visible in the XANES spectra (Fig. S3) where an increase in the white line intensity, inversely proportional to the overall Pt content, can be observed. However, this trend has to be considered only as a general qualitative indication,
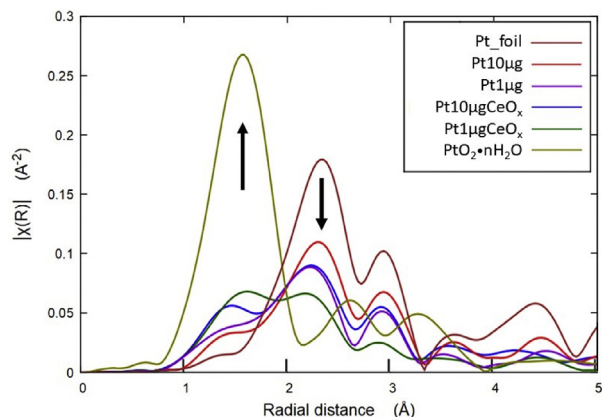
Fig. 9 − **Comparison between the k^1 Fourier transformed EXAFS spectra at the Pt L$_3$-edge of the *ex-situ* catalyst samples deposited on CIL, together with Pt foil and PtO$_2$•nH$_2$O reference compound (in this case Pt is octahedrally coordinated, but the bond-length distance is comparable to our tetrahedrally coordinated Pt).**

being a small difference and hence strongly influenced by the normalization parameters.

Our observations are in line with the previous findings of Bruix et al. [16] who compared Pt−CeO_2 anodes and observed that Pt^{2+} fraction is higher in the catalyst with lower Pt loading, which in that case was also the one with best performances. In our case, all the samples have a remarkable fraction of Pt^0 because of the reduction of the ceria substrate [16].

These findings confirm also the conclusion of Tovt et al. [18] who stated that "*when the surface O content is reduced, or Pt amount increased, the charge transfer between Pt and O is no more available and the charge transfer between Pt and Ce prevails, ultimately resulting in metallic Pt clusters exhibiting only fractional charging*".

Operando XAS at the Ce and Pt L$_3$-edge

Operando experiments were performed using a properly designed fuel cell to be used at both SAXS and XAFS beamlines of ELETTRA synchrotron.

Concerning XAS, it is worth to specify that the initial idea was to collect spectra to be analysed both in the XANES and EXAFS regions. However, after the collection of good spectra during the initial "dry" condition, before being able to run accelerated stress tests the MEA must be obviously properly hydrated with water vapours carried with the gas flow. This fact, in addition to the water generated by the cell itself, lead to the formation of water droplets onto the Kapton windows. These droplets dramatically and quickly changed the total absorption of the sample, strongly affecting the data and resulting in glitches and steps which made the spectra difficult to be properly normalized and the EXAFS part unusable (an example is provided in Fig. S4). It must be said that these measurements were conducted using the first prototype of the cell, and this problem was subsequently solved by brushing liquid Teflon on the internal surfaces of the Kapton widows (making them hydrophobic) and improving the water

Table 1 – Crystallographic data and structural parameters as obtained from the R-space fit by using the theoretical references.

Sample	%	N	Atom	R(Å)	S_0^2	R-factor	σ^2 (Å2)	ΔE_0 (eV)
Pt foil		12[a]	Pt	2.761 (13)	0.76 (5)	0.009	0.0042 (5)	7.4 (4)
Pt10 µg	0.90 (7)	12[a]	Pt	2.750 (24)	0.63 (7)	0.009	0.006 (1)	6.9 (9)
	0.10 (7)	4[b]	O	1.958 (17)			0.002 (8)	
Pt1µg	0.76 (7)	12[a]	Pt	2.730 (44)	0.68 (7)	0.008	0.007 (1)	5 (1)
	0.24 (7)	4[b]	O	1.963 (19)			0.009 (1)	
Pt10µgCeO$_x$	0.70 (5)	12[a]	Pt	2.729 (45)	0.69 (8)	0.007	0.006 (1)	4 (1)
	0.30 (5)	4[b]	O	1.941 (34)			0.006 (1)	
Pt1µgCeO$_x$	0.51 (4)	12[a]	Pt	2.733 (41)	0.77 (11)	0.010	0.008 (2)	6 (2)
	0.49 (4)	4[b]	O	1.983 (10)			0.007 (2)	

[a] Shell calculated from the crystallographic data of metallic Pt of Wyckoff (1963) [56];
[b] Shell calculated from the crystallographic data of Pt$_3$O$_4$ of Muller and Roy (1968) [57].
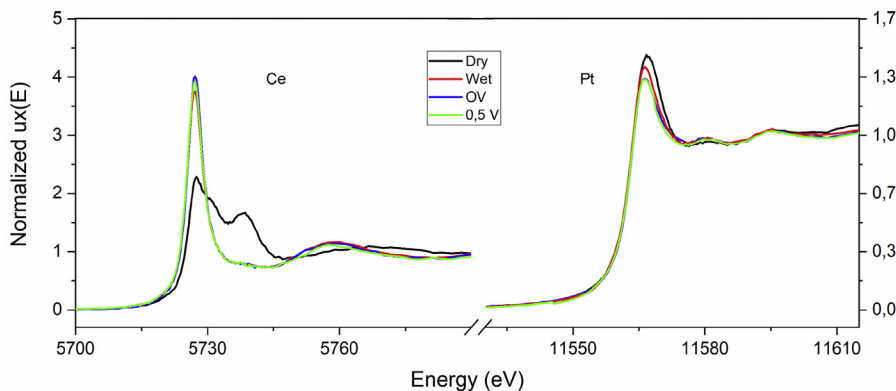
Fig. 10 – Normalized XANES spectra collected on PCC sample both at the Ce and Pt L$_3$-edges, mounted on the PEMFC in *operando* conditions. Vertical scales are different in order to better highlight the small changes in the white line of Pt spectra.

management by using lower RH, which should also improve the MEA performance [58].

The aforementioned issues did not allow to carry out a deep, time-resolved analysis. Though, it was possible to characterize the MEA in defined key stages which are representative of the MEA life cycle and of the operative conditions of the fuel cell. For these measurements, the alteration of CeO$_x$ was expected as the dissolution of anodic CeO$_x$ in PEMFC during AST is already reported in the literature by Banham et al. (2014)

[58]. Indeed, trends observed from *ex-situ* data were confirmed, as reported in Fig. 10, where it can be appreciated that the stability of Ce in PCC is even lower as it is totally (and irreversibly) reduced to Ce^{3+} just after gas flowing of humidified N$_2$, being a further confirmation of its water-driven instability.

In addition, the small changes in the white line of Pt spectra could be explained with the initial presence of mainly metallic Pt with a small fraction of Pt^{2+} which is reduced/broken or because of the reduction of the ceria support, in
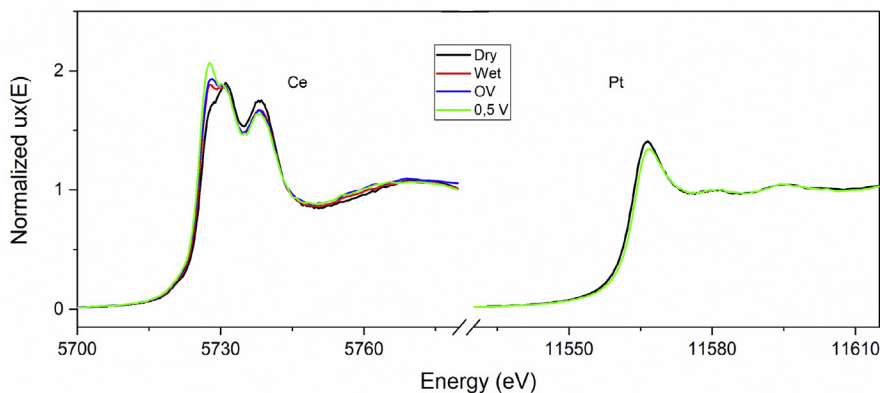
Fig. 11 – Normalized XANES spectra collected on PCnG sample both at the Ce and Pt L$_3$-edges (vertical scale is the same), mounted on the PEMFC in *operando* conditions.

agreement with Bruix et al. [16], or because of the working of the anode catalyst (as observed by Ishiguro et al. [59]), or both.

Nonetheless, the very small changes characterizing the white line only, alongside with the aforementioned problems related to the spectra normalization, makes it hard to detect and follow any Pt evolution. For this reason, Pt spectra from the MEA made up with PCnG as anode catalyst (Fig. 11), were only collected at the initial and final state of PEMFC working. Again, as already observed during *ex-situ* investigations, the Pt-CeO$_x$ catalyst directly deposited on nGDL is characterized by an higher stability than once deposited onto CIL; LCF analysis allowed to determine that the amount of Ce^{3+} in PCnG was never going above 27%. Accordingly, also the decrease in the white line of Pt spectra is less pronounced, pointing out that a Pt^{2+} fraction was still present in the catalyst.

Conclusions

In this work, two set of Pt-ceria anode catalysts sputtered on Carbon-Ionomer Layer (CIL) and on nano-Gas Diffusion Layer (nGDL) were investigated both *ex-situ* and *in operando* conditions by means of X-Ray Absorption Spectroscopy and by using a properly designed proton exchange membrane fuel cell.

Electrochemical characterization evidenced similar performances in the long-term for both systems, but the nGDL supported one show a better efficiency in the first 36 h of operation.

XANES data collected *ex-situ* at the Ce L$_3$-edge highlighted the instability of the ceria support (in air and at room temperature) when the catalyst is sputtered onto the CIL, whereas it is stable when sputtered on nGDL.

Complementary *ex-situ* EXAFS data collected on the CIL samples at the Pt L$_3$-edge evidenced also an increase in the fraction of Pt^{2+} as the overall amount of Pt (or the Pt/Ce ratio) is decreasing, in agreement with existing literature.

In preliminary test experiments conducted in *operando* using our special cell, the reduction of Ce deposited on CIL is faster as it is totally (and irreversibly) reduced to Ce^{3+} just after gas flowing of humidified N$_2$, confirming that the reaction is water-driven. On the contrary, the higher stability of nGDL catalyst is proved also in *operando*.

Our work provides useful indication about the best support to be employed for the fabrication of stable and more durable Pt-ceria catalysts for PEMFC.

Declaration of competing interest

The authors declare that they have no known competing financial interests or personal relationships that could have appeared to influence the work reported in this paper.

Acknowledgments

Appendix A. Supplementary data

Supplementary data to this article can be found online at https://doi.org/10.1016/j.ijhydene.2021.12.241.

R E F E R E N C E S

[1] Wang Y, Chen KS, Mishler J, Cho SC, Adroher XC. A review of polymer electrolyte membrane fuel cells: technology, applications, and needs on fundamental research. Appl Energy 2011;88(4):981−1007.

[2] Renner H, Schlamp G, Kleinwächter I, Drost E, Lüschow HM, Tews P, Lupton DF. Platinum group metals and compounds. Ullmann's Encycl Ind Chem 2000:1−73.

[3] Gazdzicki P, Mitzel J, Dreizler AM, Schulze M, Friedrich KA. Impact of platinum loading on performance and degradation of polymer electrolyte fuel cell electrodes studied in a rainbow stack. Fuel Cell 2018;18(3):270−8.

[4] Ostroverkh A, Johánek V, Dubau M, Kúš P, Khalakhan I, Šmíd B, Matolín V. Optimization of ionomer-free ultra-low loading Pt catalyst for anode/cathode of PEMFC via magnetron sputtering. Int J Hydrogen Energy 2019;44(35):19344−56.

[5] Yakovlev YV, Nováková J, Kúš P, Dinhová TN, Matolínová I, Matolín V. Highly developed nanostructuring of polymer-electrolyte membrane supported catalysts for hydrogen fuel cell application. J Power Sources 2019;439:227084.

[6] Yu X, Ye S. Recent advances in activity and durability enhancement of Pt/C catalytic cathode in PEMFC: Part I. Physico-chemical and electronic interaction between Pt and carbon support, and activity enhancement of Pt/C catalyst. J Power Sources 2007;172(1):133−44.

[7] Khalakhan I, Supik L, Vorokhta M, Yakovlev Y, Dopita M, Sandbeck DJS, Matolínová I. Compositionally tuned magnetron co-sputtered PtxNi100-x alloy as a cathode catalyst for proton exchange membrane fuel cells. Appl Surf Sci 2020;511:145486.

[8] Kúš P, Ostroverkh A, Khalakhan I, Fiala R, Kosto Y, Šmíd B, Matolín V. Magnetron sputtered thin-film vertically segmented Pt-Ir catalyst supported on TiC for anode side of proton exchange membrane unitized regenerative fuel cells. Int J Hydrogen Energy 2019;44(31):16087−98.

[9] Trovarelli A, Fornasiero P. Catalysis by ceria and related materials. Singapore: World Scientific; 2013. ed. 2nd.

[10] Mullins DR. The surface chemistry of cerium oxide. Surf Sci Rep 2015;70:42−85.

[11] Pongpichayakul N, Themsirimongkon S, Maturost S, Wangkawong K, Fang L, Inceesungvorn B, Saipanya S. Cerium oxide-modified surfaces of several carbons as supports for a platinum-based anode electrode for methanol electro-oxidation. Int J Hydrogen Energy 2021;46(3):2905−16.

[12] Gandhi HS, Graham GW, McCabe RW. Automotive exhaust catalysis. J Catal 2003;216:433−42.

[13] Burlakovs J, Vincevica-Gaile Z, Krievans M, Jani Y, Horttanainen M, Pehme KM, Klavins M. Platinum group elements in geosphere and anthroposphere: interplay among the global reserves, urban ores, markets and circular economy. Minerals 2020;10(6):558.

[14] Fu Q, Saltsburg H, Flytzani-Stephanopoulos M. Active nonmetallic Au and Pt species on ceriabased water-gas shift catalysts. Science 2003;301:935—8.

[15] Fiala R, Khalakhan I, Matolinova I, Vaclavu M, Vorokhta M, Sofer Z, Huber S, Potin V, Matolin V. Pt-CeO$_2$ coating of carbon nanotubes grown on anode gas diffusion layer of the polymer electrolyte membrane fuel cell. J Nanosci Nanotechnol 2011;11(6):5062—7.

[16] Bruix A, Lykhach Y, Matolínová I, Neitzel A, Skála T, Tsud N, Fiala R. Maximum noble-metal efficiency in catalytic materials: atomically dispersed surface platinum. Angew Chem Int Ed 2014;53(39):10525—30.

[17] Matolin V, et al. Platinum-doped CeO2 thin film catalysts prepared by magnetron sputtering. Langmuir 2010;26:12824—31.

[18] Tovt A, Bagolini L, Dvořák F, Tran ND, Vorokhta M, Beranová K, Mysliveček J. Ultimate dispersion of metallic and ionic platinum on ceria. J Mater Chem 2019;7(21):13019—28.

[19] V. Matolin, Method for preparing oxidation catalyst and catalyst prepared by the oxidation.

[20] Matolin V, et al. Pt and Sn doped sputtered CeO2 electrodes for fuel cell applications. Fuel Cell 2010;10:139—44.

[21] Fiala R, et al. Proton exchange membrane fuel cell made of magnetron sputtered Pt—CeOx and Pt—Co thin film catalysts. J Power Sources 2015;273:105—9.

[22] Fiala R, Vaclavu M, Rednyk A, Khalakhan I, Vorokhta M, Lavkova J, Potin V, Matolinova I, Matolin V. Pt—CeOx thin film catalysts for PEMFC. Catal Today 2015;240 Part B(1 Feb):236—41.

[23] Wang Y, Diaz DFR, Chen KS, Wang Z, Adroher XC. Materials, technological status, and fundamentals of PEM fuel cells—a review. Mater Today 2020;32:178—203.

[24] Dvořák F, et al. Creating single-atom Pt-ceria catalysts by surface step decoration. Nat Commun 2016;7:10801.

[25] Yang X, et al. Single-atom catalysts: a new frontier in heterogeneous catalysis. Acc Chem Res 2013;46:1740—8.

[26] Flytzani-Stephanopoulos M, Gates BC. Atomically dispersed supported metal catalysts. Annu Rev Chem Biomol Eng 2012;3:545—74.

[27] Hatanaka M, et al. Ideal Pt loading for a Pt/CeO$_2$-based catalyst stabilized by a Pt—O—Ce bond. Appl Catal B Environ 2010;99:336—42.

[28] Moses-DeBusk M, et al. CO oxidation on supported single Pt atoms: experimental and ab initio density functional studies of CO interaction with Pt atom on θ-Al2O3(010) surface. J Am Chem Soc 2013;135:12634—45.

[29] Narula CK, Allard LF, Stocks GM, Moses-DeBusk M. Remarkable NO oxidation on single supported platinum atoms. Sci Rep 2014;4:7238.

[30] Ding K, et al. Identification of active sites in CO oxidation and water-gas shift over supported Pt catalysts. Science 2015;350:189—92.

[31] Kopelent R, van Bokhoven JA, Szlachetko J, Edebeli J, Paun C. Catalytically active and spectator Ce3+ in ceria-supported metal catalysts. Angew Chem 2015;127(30):8852—5.

[32] Newton MA, Ferri D, Smolentsev G, Marchionni V, Nachtegaal M. Room-temperature carbon monoxide oxidation by oxygen over Pt/Al2O3 mediated by reactive platinum carbonates. Nat Commun 2015;6:8675.

[33] Fiala R, Figueroba A, Bruix A, Vaclavu M, Rednyk A, Khalakhan I, Vorokhta M, Lavkova J, Illas F, Potin V, Matolinova I, Neyman KM, Matolin V. High efficiency of Pt^{2+}- CeO$_2$ novel thin film catalyst as anode for proton exchange membrane fuel cells Appl. Appl Catal B: Environ 2016;197(15 Nov):262—70.

[34] Nováková J, Dubau M, Fuka Š, Duchoň T, Johánek V, Fiala R, Matolínová I. Role of nitrogenated carbon in tuning Pt-CeOx based anode catalysts for higher performance of hydrogen-powered fuel cells. Appl Surf Sci 2020;515:146054.

[35] Amenitsh H, Rappolt M, Kriechbaum M, Mio H, Laggner P, Bernstorff S. First performance assessment of the small-angle X-ray scattering beamline at ELETTRA. J Synchrotron Radiat 1998;5(3):506—8.

[36] Burian M, Meisenbichler C, Naumenko D, Amenitsch H. SAXSDOG: open software for real-time azimuthal integration of 2D scattering images. arXiv 2020;2007:2022.

[37] Gebel G, Diat O. Neutron and X-ray scattering: suitable tools for studying ionomer membranes. Fuel Cell 2005;5(2):261—76.

[38] Kotlarchyk M, Chen SH. Analysis of small angle neutron scattering spectra from polydisperse interacting colloids. J Chem Phys 1983;79(5):2461—9.

[39] Kotlarchyk M, Stephens RB, Huang JS. Study of Schultz distribution to model polydispersity of microemulsion droplets. J Phys Chem 1988;92(6):1533—8.

[40] Sharma RV, Sharma KC. The structure factor and the transport properties of dense fluids having molecules with square well potential, a possible generalization. Phys Stat Mech Appl 1977;89(1):213—8.

[41] Pontoni D, Finet S, Narayanan T, Rennie AR. Interactions and kinetic arrest in an adhesive hard-sphere colloidal system. J Chem Phys 2003;119(12):6157—65.

[42] Di Cicco A, Aquilanti G, Minicucci M, Principi E, Novello N, Cognigni A, Olivi L. J Phys Conf Ser 2009;190(1):12043.

[43] Karydas AG, Czyzycki M, Leani JJ, Migliori A, Osan J, Bogovac M, Gol MG. An IAEA multi-technique X-ray spectrometry endstation at Elettra Sincrotrone Trieste: benchmarking results and interdisciplinary applications. J Synchrotron Radiat 2018;25(1):189—203.

[44] Jark W, Eichert D, Luehl L, Gambitta A. Optimisation of a compact optical system for the beam transport at the x-ray fluorescence beamline at Elettra for experiments with small spots. In: Advances in X-ray/EUV optics and components IX, vol. 9207. International Society for Optics and Photonics; 2014, September. 92070G.

[45] Ravel B, Newville M. J Synchrotron Radiat 2005;12:537—41.

[46] Newville M. IFEFFIT: interactive XAFS analysis and FEFF fitting. J Synchrotron Radiat 2001;8:322—4.

[47] Wells PP, Crabb EM, King CR, Fiddy S, Amieiro-Fonseca A, Thompsett D, Russell AE. Reduction properties of Ce in CeOx/Pt/Al$_2$O$_3$ catalysts. Catal Struct React 2015;1(2):88—94.

[48] Hayes SA, Yu P, O'Keefe TJ, O'Keefe MJ, Stoffer JO. The phase stability of cerium species in aqueous systems: I. E-pH diagram for the system. J Electrochem Soc 2002;149(12):C623.

[49] Grulke E, Reed K, Beck M, Huang X, Cormack A, Seal S. Nanoceria: factors affecting its pro-and anti-oxidant properties. Environ Sci: Nano 2014;1(5):429—44.

[50] Channei D, Phanichphant S, Nakaruk A, Mofarah SS, Koshy P, Sorrell CC. Aqueous and surface chemistries of photocatalytic Fe-doped CeO2 nanoparticles. Catalysts 2017;7(2):45.

[51] Yu P, Hayes SA, O'Keefe TJ, O'Keefe MJ, Stoffer JO. The phase stability of cerium species in aqueous systems: II. The systems. Equilibrium considerations and pourbaix diagram calculations. J Electrochem Soc 2005;153(1):C74.

[52] Baker AM, Wang L, Johnson WB, Prasad AK, Advani SG. Nafion membranes reinforced with ceria-coated multiwall carbon nanotubes for improved mechanical and chemical durability in polymer electrolyte membrane fuel cells. J Phys Chem C 2014;118(46):26796—802.

[53] Benziger J, Nehlsen J, Blackwell D, Brennan T, Itescu J. Water flow in the gas diffusion layer of PEM fuel cells. J Membr Sci 2005;261(1−2):98−106.

[54] Schulz VP, Becker J, Wiegmann A, Mukherjee PP, Wang CY. Modeling of two-phase behavior in the gas diffusion medium of PEFCs via full morphology approach. J Electrochem Soc 2007;154(4):B419.

[55] Sinha PK, Wang CY. Liquid water transport in a mixed-wet gas diffusion layer of a polymer electrolyte fuel cell. Chem Eng Sci 2008;63(4):1081−91.

[56] Wyckoff RWG. Crystal structures 1. American Mineralogist Crystal Structure Database; 1963. p. 7−83.

[57] Muller O, Roy R. Formation and stability of the platinum and rhodium oxides at high oxygen pressures and the structures of Pt_3O_4, β-PtO_2 and RhO_2. J Less Common Met 1968;16(2):129−46.

[58] Banham D, Ye S, Cheng T, Knights S, Stewart SM, Wilson M, Garzon F. Effect of ceox crystallite size on the chemical stability of ceox nanoparticles. J Electrochem Soc 2014;161(10):F1075.

[59] Ishiguro N, Kityakarn S, Sekizawa O, Uruga T, Matsui H, Taguchi M, Tada M. Kinetics and mechanism of redox processes of Pt/C and Pt3Co/C cathode electrocatalysts in a polymer electrolyte fuel cell during an accelerated durability test. J Phys Chem C 2016;120(35):19642−51.